ChemComm

COMMUNICATION

View Article Online
View Journal | View Issue

Cite this: *Chem. Commun.*, 2024, **60**, 14200

Received 27th September 2024,
Accepted 6th November 2024

DOI: 10.1039/d4cc05037a

rsc.li/chemcomm

Origin of anisotropic thermal transport in $CsPbBr_3$†

Wilarachchige D. C. B. Gunatilleke, * Oluwagbemiga P. Ojo and George S. Nolas

We reveal the specific structural and bonding features that result in anisotropic thermal transport for $CsPbBr_3$ by directional single-crystal measurements and elucidate the bases for the low Debye temperature and speed of sound. This work enhances the research on perovskites and reveals the structural features governing the thermal properties.

Perovskites are a broad class of materials with different structure types and compositions, and continue to be of scientific interest as well as of technological importance for a diverse range of applications including solar-cell absorbers,[1–3] photocatalysts for solar water splitting,[4,5] nonlinear optics,[6,7] radiation detection,[8,9] topological insulators,[10] thermoelectrics,[11] magneto-optic and magneto-ferroics.[12,13] This is primarily due to continued advances in synthetic chemistry and characterization techniques that allow for an understanding of the structure–property relationships that govern the different physical properties of interest.

In advancing our fundamental understanding of the perovskite materials currently of interest, whether reports of new materials with superior properties have been published or if advances towards device development have been initiated, an in-depth understanding of the thermal properties is of paramount importance for any application of interest.[14,15] Moreover, specific structural features and related scattering mechanisms can directly affect the thermal properties of crystalline solids. For example, a complex lattice accommodating many atoms, and atoms of differing size and mass, will affect the thermal transport.[16,17] Anharmonic processes associated with the crystal structure are intrinsic to the lattice and directly affect bonding and therefore thermal properties.[18–20] Directional and structural variations can also significantly affect thermal properties.[18] Thus, an understanding of such effects is essential in developing a fundamental understanding of the thermal properties of any crystalline solid.

The perovskite $CsPbBr_3$ has been investigated as a high-performance radiation detector.[21,22] It has also been reported to possess low thermal conductivity above room temperature making it of interest for thermoelectric applications.[23,24] This is not surprising, given the heavy constituent atoms as well as soft modes that contribute to enhanced phonon scattering within the crystal lattice.[25] Nevertheless, an in-depth investigation of the thermal properties and understanding the anisotropic thermal transport, not previously reported to the best of our knowledge, has not been undertaken. Herein we investigate the thermal properties of single-crystal orthorhombic (*Pnma*) $CsPbBr_3$. In addition to analysis of the directional temperature-dependent thermal conductivity, κ, we investigate and model the specific heat, C_p, and evaluate the Debye temperature, θ_D, speed-of-sound, υ, and anharmonicity in providing insight into the origins of the thermal properties as well as the structural and bonding features that result in the anisotropic thermal transport and ultra-low thermal conductivity this material possesses. There have been several theoretical investigations regarding the origins of the lattice anharmonicity in $CsPbBr_3$, and we utilize this work in our analyses. Nevertheless, these theoretical investigations utilize κ data from $CsPbBr_3$ nanowires,[26] and in this work, directional single-crystal thermal transport was investigated to determine the anisotropic κ and anharmonicity in addition to the intrinsic thermal properties of this material.

The perovskite crystal structure of $CsPbBr_3$ (Fig. 1) consists of chains of corner sharing $Pb–Br1_2Br2_4$ octahedra rotated on the *a*–*b* plane and tilted out-of-phase away from the *c*-axis compared to the tetragonal phase that exists above 361 K,[27] providing $CsPbBr_3$ with unique structural and vibrational properties as described below.[28] The arrangement of Pb–Br–Pb chains forms a three-dimensional network of anion cages that consists of corner sharing octahedra capable of encompassing Cs^+ in an environment formed by four Br1 and eight Br2. The Cs atoms are loosely bonded to Br with highly varying bond distances and occupy the void spaces between the octahedra with strong polar covalent bonds between Pb and Br.[29] Such an arrangement may result in significant bonding heterogeneity.

Department of Physics, University of South Florida, Tampa, FL 33620, USA. E-mail: gnolas@usf.edu

† Electronic supplementary information (ESI) available. See DOI: https://doi.org/10.1039/d4cc05037a

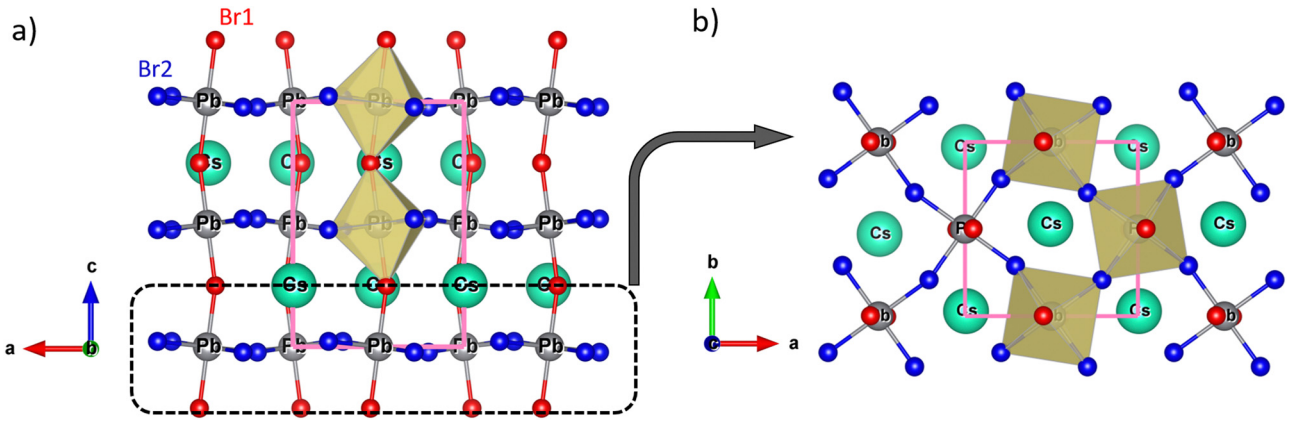

Fig. 1 Crystal structure of $CsPbBr_3$ highlighting the (a) out-of-phase tilting and (b) in-phase tilting of $PbBr_6$ octahedra. The unit cell is marked with a solid pink line.

Furthermore, the out-of-phase tilting of the octahedra will influence the thermal properties of $CsPbBr_3$ under different temperature regimes. Moreover, the octahedral tilting increases with decreasing temperature and the structure distortion due to octahedral rotation results in negative thermal expansion of the *b* lattice parameter of the unit cell.[30] Below 10 K the structure distortion reaches a limit in the octahedral rotation, thus an inconsistent variation of the lattice constants is observed.[30]

Fig. 2 shows the directions of κ measurements with respect to the crystal structure and associated crystallographic planes. The Pb–Br1–Pb chains lie on the *a*–*c* plane, that is perpendicular to the (204) plane, as shown in Fig. 1(a). However, the Pb–Br2–Pb chains do not lie on the same plane. The out-of-plane tilting of $PbBr_6$ octahedra away from the *c*-axis leads to tilting of the Pb–Br2–Pb chains above and below the *a*–*b* plane, *i.e.*, 18.78°–29.73° away from the (204) plane. As shown in Fig. 3, there is large anisotropy in κ with an increase in the anisotropy in κ along the measured directions at lower temperatures, *i.e.*, κ measured parallel to (204) is significantly higher than that along the direction perpendicular to (204). This suggests that the Pb–Br1–Pb chains (characterized by out-of-phase tilted $PbBr_6$ octahedra) play an important role in thermal transport

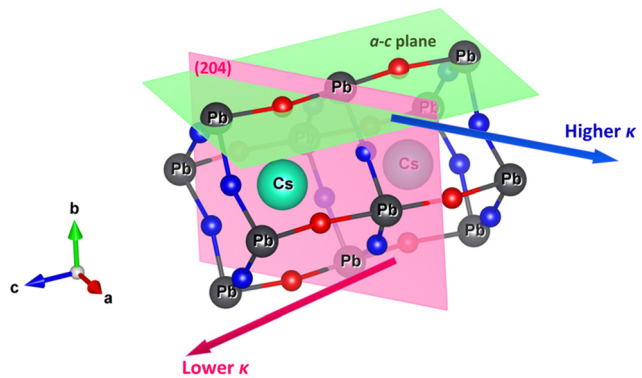

Fig. 2 Orientation of the (204) crystallographic plane with respect to the crystal structure of $CsPbBr_3$ and the directions of the measurements of κ.

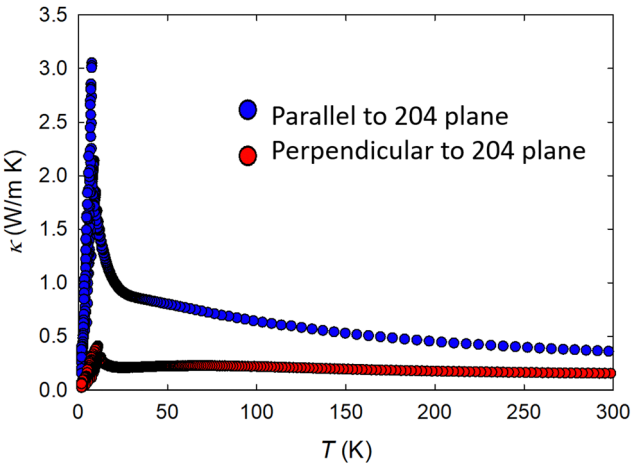

Fig. 3 Temperature dependent κ data parallel (blue) and perpendicular (red) to the (204) plane.

perpendicular to the (204) plane resulting in ultra-low κ while Pb–Br2–Pb chains dominate that parallel to the (204) plane (characterized by in-phase tilted $PbBr_6$ octahedra) leading to comparatively higher κ. Very recently it was reported that the low frequency modes that correspond to out-of-phase tilting of the $PbBr_6$ octahedra are at a significantly lower frequency range than those that correspond to in-plane-tilting.[28] This correlates with the lower κ values perpendicular to the (204) plane at low temperatures, and is attributable to enhanced phonon scattering by these low frequency modes resulting from the out-of-phase tilting of the octahedra. At higher temperatures, particularly near room temperature, there exists anisotropy in thermal transport along both directions. However, the effect of low-frequency modes on thermal transport at high temperatures may not be as dominant as they are at low temperatures. Our structural analyses (see ESI†) provide insight to the observed anisotropy in thermal properties. These results emphasize the importance of thermal displacement of the octahedral framework at high temperatures on the thermal transport, and are in agreement with the analyses by Songvilay *et al.*[31] At 300 K the

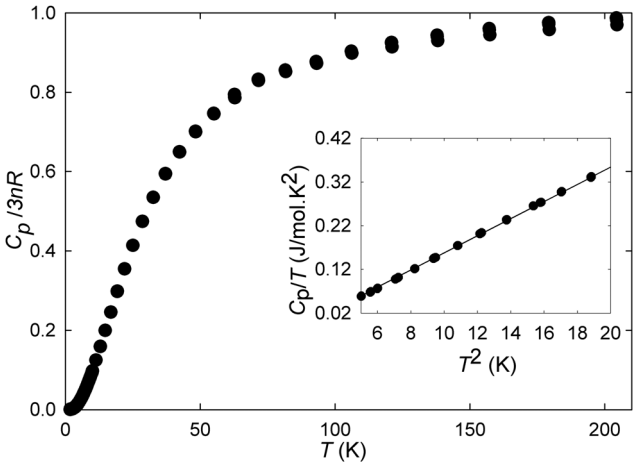

Fig. 4 Temperature dependent C_p data. The inset shows the low temperature data fit of the for C_p/T *vs.* T^2.

anisotropic atomic displacement parameters, U_{ij}, for Br1 and Br2 are significantly large along certain directions compared to the other directions. Specifically, the U_{11} = 0.141 (7) Å and U_{22} = 0.163 (7) Å for Br1 correspond to atomic displacements along the *ab*-plane that are significantly larger than the atomic displacements on the *c*-axis (U_{33} = 0.0282 (25)). In contrast, U_{11} = 0.072 (29) Å and U_{22} = 0.0687 (30) Å for Br2 are smaller than U_{33} = 0.122 (4) Å indicating larger atomic displacements along the *c*-axis compared to those along the *ab*-plane. However, the difference between U_{33} and U_{11} or U_{22} for Br2 is not as large as that for Br1, leading to ultra-low κ perpendicular to the (204) plane. Nevertheless, the relatively large U_{ij} values for Br2 result in low κ parallel to (204) plane, as shown in Fig. 3.

To further investigate the thermal properties of $CsPbBr_3$, we investigated temperature dependent C_p, as shown in Fig. 4. The C_p data approach the Dulong–Petit limit above 100 K indicating that the majority of acoustic and optic mode frequencies are excited at this relatively low temperature. The solid line in the inset of Fig. 4 is a linear fit to the low temperature data, modeled by the equation $C_p = \alpha T + \beta T^3$, where the first and second terms represent the Sommerfeld coefficient and the lattice contribution, respectively.[32] Using the relation $\theta_D = (12\pi^4 R n_a/5\beta)^{1/3}$, θ_D can be determined from the low temperature C_p data, where n_a is the number of atoms per formula unit and R is the universal gas constant. A value of 80 K for θ_D was obtained from the data fit. The average speed of sound (υ = 914 m s^{-1}) was obtained using the relation $\theta_D = \upsilon(h/k_B)(3n_aN_ad/4\pi M_w)^{1/3}$, where h is Planck's constant, k_B is the Boltzmann constant, N_a is Avogadro's constant, d is the density, and M_w is the molecular weight. The value for υ is low, in reasonable agreement with a previously reported value,[33] and is indicative of the weak bonding interactions within the crystalline lattice possibly due to the tilting of the $PbBr_6$ octahedra leading to asymmetric bonding around the cation sites. For insulators or large bandgap semiconductors where the lattice contribution to κ dominates phonon transport, κ is related to the Grüneisen parameter, γ, by $\kappa = BMV^{1/3}/\theta_D{}^3/n^2/3\gamma^2T$, where $B = 2.43 \times 10^{-8}/(1–0.514/\gamma + 0.228/\gamma^2)$, M is the average mass of an atom in the crystal (amu), V is the volume of the unit cell, n is the number of atoms per primitive cell, and T is absolute temperature.[34–36] The obtained room temperature γ values of 2.13 and 1.38 perpendicular and parallel to (204) plane, respectively, indicate large anisotropy in the anharmonicity. *Ab initio* simulations performed by Sadok *et al.*[37] indicated large anisotropy between the longitudinal and transverse speed of sound in $CsPbBr_3$. This anisotropy in lattice anharmonicity due to the in-plane and out-of-plane tilting of $PbBr_6$ octahedra, as well as the weak interactions of the Cs cations within the voids of $PbBr_6$ octahedral sublattice,[37] can lead to the anisotropic properties in the lattice.

In summary, a large single crystal, grown from the melt using optimized Bridgman growth conditions, was used to investigate the origins of anisotropic thermal transport in $CsPbBr_3$. The κ measured in the parallel and perpendicular directions relative to the (204) plane indicated large anisotropy in the thermal transport. The difference in κ along the two directions significantly increases at lower temperatures. The alignment of Pb–Br1–Pb chains predominantly perpendicular to the (204) plane leads to low-frequency modes resulting from out-of-phase tilted $PbBr_6$ octahedra,[33,35] which contribute to phonon scattering, particularly at low temperatures, giving rise to large anisotropy in the thermal transport. The low values for θ_D and υ indicate relatively weak bonding, an observation that is in accord with the specific bonding nature of Pb–Br and Cs–Br, and in agreement with theoretically predicted values for $CsPbBr_3$.[38] Moreover, there is anisotropy in the lattice anharmonicity perpendicular and parallel to the (204) plane, supporting these findings.

Wilarachchige D. C. B. Gunatilleke: data curation, investigation, formal analysis, visualization, writing – original draft. Oluwagbemiga P. Ojo: data curation, investigation, formal analysis. George S. Nolas: conceptualization, investigation, supervision, writing – review & editing, project administration.

The authors gratefully acknowledge support from Amethyst Research, Inc., USA.

Data availability

The data supporting this article have been included as part of the ESI.†

Conflicts of interest

There are no conflicts to declare.

References

1 Q. Xu, D. Yang, J. Lv, Y.-Y. Sun and L. Zhang, *Small Methods*, 2018, **2**, 1700316.
2 A. Krishna, S. Gottis, M. K. Nazeeruddin and F. Sauvage, *Adv. Funct. Mater.*, 2019, **29**, 1806482.
3 C. Ortiz-Cervantes, P. Carmona-Monroy and D. Solis-Ibarra, *ChemSusChem*, 2019, **12**, 1560–1575.
4 Y. Huang, J. Liu, Y. Deng, Y. Qian, X. Jia, M. Ma, C. Yang, K. Liu, Z. Wang, S. Qu and Z. Wang, *J. Semicond.*, 2020, **41**, 011701.

5 G. Zhang, G. Liu, L. Wang and J. T. S. Irvine, *Chem. Soc. Rev.*, 2016, **45**, 5951–5984.
6 J. Xu, X. Li, J. Xiong, C. Yuan, S. Semin, T. Rasing and X.-H. Bu, *Adv. Mater.*, 2020, **32**, 1806736.
7 Y. Zhou, Y. Huang, X. Xu, Z. Fan, J. B. Khurgin and Q. Xiong, *Appl. Phys. Rev.*, 2020, **7**, 041313.
8 G. Kakavelakis, M. Gedda, A. Panagiotopoulos, E. Kymakis, T. D. Anthopoulos and K. Petridis, *Adv. Sci.*, 2020, **7**, 2002098.
9 K. R. Dudipala, T.-H. Le, W. Nie and R. L. Z. Hoye, *Adv. Mater.*, 2024, **36**, 2304523.
10 H. Wei, C. Yang, Y. Wu, B. Cao, M. Lorenz and M. Grundmann, *J. Mater. Chem. C*, 2020, **8**, 15575–15596.
11 M. A. Haque, S. Kee, D. R. Villalva, W.-L. Ong and D. Baran, *Adv. Sci.*, 2020, **7**, 1903389.
12 J. P. Velev, S. S. Jaswal and E. Y. Tsymbal, *Philos. Trans. R. Soc., A*, 2011, **369**, 3069–3097.
13 Y. Lv, Y. Wang, X. Ma, Y. Xu, L. Wang, X. Wang, M. Xiao and C. Zhang, *Adv. Phys.: X*, 2023, **8**, 2258951.
14 A. K. Roy, B. L. Farmer, V. Varshney, S. Sihn, J. Lee and S. Ganguli, *ACS Appl. Mater. Interfaces*, 2012, **4**, 545–563.
15 Y. Lin, Y. Jia, G. Alva and G. Fang, *Renewable Sustainable Energy Rev.*, 2018, **82**, 2730–2742.
16 G. S. Nolas and H. J. Goldsmid, in *Thermal Conductivity*, ed. T. M. Tritt, Springer, US, 2004, pp. 105–121.
17 W. D. C. B. Gunatilleke, A. F. May, H. Wang and G. S. Nolas, *Appl. Phys. Lett.*, 2020, **117**, 092101.
18 T. Ghosh, M. Dutta, D. Sarkar and K. Biswas, *J. Am. Chem. Soc.*, 2022, **144**, 10099–10118.
19 G. S. Nolas, G. Fowler and J. Yang, *J. Appl. Phys.*, 2006, **100**, 043705.
20 Y. Dong, A. R. Khabibullin, K. Wei, J. R. Salvador, G. S. Nolas and L. M. Woods, *Chem. Phys. Chem.*, 2015, **16**, 3264–3270.
21 Y. He, L. Matei, H. J. Jung, K. M. McCall, M. Chen, C. C. Stoumpos, Z. Liu, J. A. Peters, D. Y. Chung, B. W. Wessels, M. R. Wasielewski, V. P. Dravid, A. Burger and M. G. Kanatzidis, *Nat. Commun.*, 2018, **9**, 1609.
22 L. Pan, Z. Liu, C. Welton, V. V. Klepov, J. A. Peters, M. C. De Siena, A. Benadia, I. Pandey, A. Miceli, D. Y. Chung, G. N. M. Reddy, B. W. Wessels and M. G. Kanatzidis, *Adv. Mater.*, 2023, **35**, 2211840.
23 Z. Yao, W. Cao, Z. Wang, L. Miao, J. Shi and R. Xiong, *Phys. Chem. Chem. Phys.*, 2023, **25**, 26236–26244.
24 X. Wang, Z. Gao, G. Zhu, J. Ren, L. Hu, J. Sun, X. Ding, Y. Xia and B. Li, *Phys. Rev. B*, 2023, **107**, 214308.
25 T. Lanigan-Atkins, X. He, M. J. Krogstad, D. M. Pajerowski, D. L. Abernathy, G. N. M. N. Xu, Z. Xu, D.-Y. Chung, M. G. Kanatzidis, S. Rosenkranz, R. Osborn and O. Delaire, *Nat. Mater.*, 2021, **20**, 977–983.
26 W. Lee, H. Li, A. B. Wong, D. Zhang, M. Lai, Y. Yu, Q. Kong, E. Lin, J. J. Urban, J. C. Grossman and P. Yang, *Proc. Natl. Acad. Sci. U. S. A.*, 2017, **114**, 8693–8697.
27 C. C. Stoumpos, C. D. Malliakas, J. A. Peters, Z. Liu, M. Sebastian, J. Im, T. C. Chasapis, A. C. Wibowo, D. Y. Chung, A. J. Freeman, B. W. Wessels and M. G. Kanatzidis, *Cryst. Growth Des.*, 2013, **13**, 2722–2727.
28 A. E. J. Hoffman, R. A. Saha, S. Borgmans, P. Puech, T. Braeckevelt, M. B. J. Roeffaers, J. A. Steele, J. Hofkens and V. Van Speybroeck, *APL Mater.*, 2023, **11**, 41124.
29 S. Thakur and A. Giri, *ACS Appl. Mater. Interfaces*, 2023, **15**, 26755–26765.
30 C. A. López, C. Abia, M. C. Alvarez-Galván, B.-K. Hong, M. V. Martínez-Huerta, F. Serrano-Sánchez, F. Carrascoso, A. Castellanos-Gómez, M. T. Fernández-Díaz and J. A. Alonso, *ACS Omega*, 2020, **5**, 5931–5938.
31 M. Songvilay, N. Giles-Donovan, M. Bari, Z.-G. Ye, J. L. Minns, M. A. Green, G. Xu, P. M. Gehring, K. Schmalzl, W. D. Ratcliff, C. M. Brown, D. Chernyshov, W. van Beek, S. Cochran and C. Stock, *Phys. Rev. Mater.*, 2019, **3**, 093602.
32 C. Kittel and P. McEuen, *Introduction to Solid State Physics*, John Wiley & Sons, 2018.
33 G. A. Elbaz, W.-L. Ong, E. A. Doud, P. Kim, D. W. Paley, X. Roy and J. A. Malen, *Nano Lett.*, 2017, **17**, 5734–5739.
34 D. T. Morelli and G. A. Slack, in *High Thermal Conductivity Materials*, ed. S. L. Shindé and J. S. Goela, Springer, New York, NY, 2006, pp. 37–68.
35 G. A. Slack, in *Solid State Physics*, eds. H. Ehrenreich, F. Seitz and D. Turnbull, Academic Press, 1979, vol. 34, pp. 1–71.
36 C. L. Julian, *Phys. Rev.*, 1965, **137**, A128–A137.
37 R. Ben Sadok, A. Muñoz, P. Rodríguez-Hernández, H. Djani and D. Hammoutène, *J. Solid State Chem.*, 2022, **314**, 123402.
38 F. Bridges, J. Gruzdas, C. MacKeen, K. Mayford, N. J. Weadock, V. U. Baltazar, Y. Rakita, L. Waquier, J. A. Vigil, H. I. Karunadasa and M. F. Toney, *Phys. Rev. B*, 2023, **108**, 214102.